AIAA JOURNAL
Vol. 30, No. 8, August 1992

Computation of Turbulent, Separated, Unswept Compression Ramp Interactions

T. A. Marshall* and D. S. Dolling†
University of Texas at Austin, Austin, Texas 78712

Examination of the literature shows that the comparison between experiment and computation for highly separated unswept compression ramp flows is generally poor, irrespective of the turbulence model used. In general, the upstream influence is not correct, the wall pressure rise through separation is too steep, and the pressures under the separated shear layer are too high. In the current study, the objective is to determine if these discrepancies might be attributed more to other factors such as flowfield unsteadiness or three-dimensionality, rather than to inadequate turbulence modeling. To examine this possibility, multichannel wall pressure fluctuations were measured under the unsteady separation shock wave in a 28 deg unswept compression ramp flow at Mach 5. The results show that the large scale, low frequency separation shock unsteadiness controls the distribution of time-averaged surface properties and that neglect of the unsteadiness is probably the primary cause of the discrepancy between experiment and computation.

Introduction

SHOCK-wave/boundary-layer interactions have been the subject of much research over the past thirty years. They commonly occur on high speed aircraft and missiles and can generate large aerodynamic loads and heat transfer rates, particularly if separation occurs. For this reason, among others, these phenomena must be understood better and the study of them remains an important research area. It is highly unlikely that such flowfields will ever be solved analytically. As a result, progress depends heavily upon computational modeling and experiment.

Numerical methods have now reached the stage where solutions for several types of separated interactions agree reasonably well with experiment. These include three-dimensional flows induced by sharp fins at angle of attack,[1,2] by blunt fins with hemicylindrical leading edges,[3,4], and by swept compression ramps.[5,6] Although few detailed comparisons have been made with measurements of such sensitive parameters as wall shear stress or heat transfer rate, the computations generally predict quite well the wall pressures, pertinent interaction length scales and angles, and the main features of the separated flow structure and external inviscid flowfield. In contrast, and somewhat surprisingly, two-dimensional flows such as those generated by unswept compression ramps, have proved more difficult to predict.[7-10] For the two-dimensional cases there seems to be three likely causes for the discrepancy between computation and experiment: 1) inadequate turbulence modeling; 2) interaction unsteadiness; and 3) the assumption that the flow is two-dimensional. Any one, or some combination of them may be the cause of the poor comparison with experiment. Some brief remarks about each are given below.

Turbulence Modeling

Numerous computations, using a variety of turbulence models, have been made of the 24 deg Mach 3 unswept compression ramp experiment of Settles.[11] Three sets of computed wall pressure distributions for this flow are shown in Fig. 1. Figure 1a shows those calculated by Viegas and Horstman[7] using turbulence models available in 1979, Fig. 1b shows the results of Champney[9] presented in 1989 using more recent turbulence models, while Fig. 1c shows the most recent computations by Wilcox[10] using the new "multiscale" model and the $k-\omega$ model. Champney's[9] work includes calculations made using the turbulence model of Mansour and Shih, which was derived from direct simulation data for a channel flow and is applied for the first time to a compressible flow by

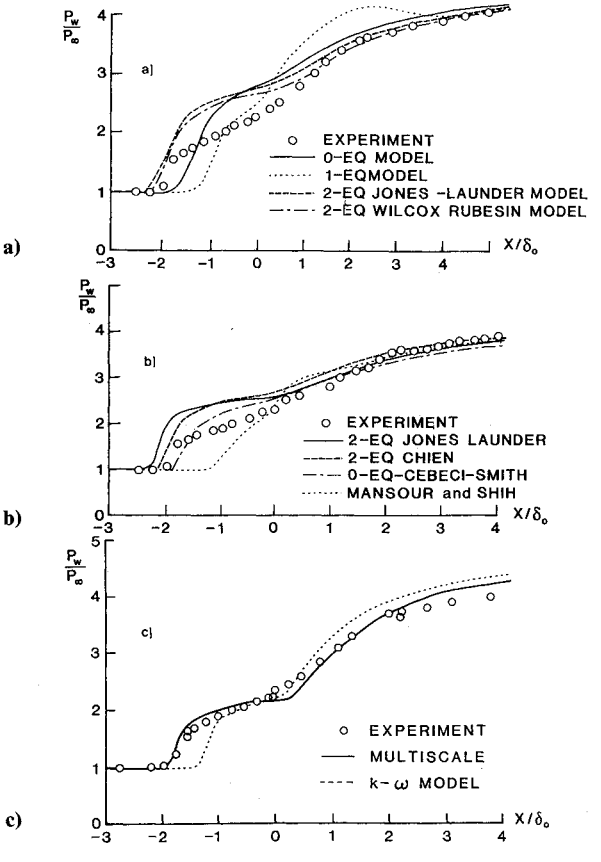

Fig. 1 Measured and computed wall pressure distributions in a 24-deg, Mach 3 compression ramp interaction: a) Viegas and Horstman, 1979, Ref. 7; b) Champney, 1989, Ref. 9; c) Wilcox, 1990, Ref. 10.

Received Aug. 2, 1990; revision received Oct. 7, 1991; accepted for publication Nov. 29, 1991.

*Graduate Student, currently Associate Engineer, Lockheed Engineering and Sciences Co., 2400 NASA Road 1, Houston, TX 77058. Member AIAA.

†Associate Professor, Associate Fellow AIAA.

Champney.[9] Full details are given in Ref. 9. The computations in Figs. 1a and 1b all share a common feature—a much steeper pressure gradient up through separation to the corner and a substantially higher "plateau" level upstream of the corner than in the experiment. In contrast, the $k-\omega$ model in Fig. 1c predicts the plateau pressure fairly well, but the upstream influence is substantially underpredicted. Of all the computations, Wilcox's[10] multiscale model is clearly superior; both upstream influence and plateau pressure levels are predicted well. The multiscale model does employ a more realistic physical description of the Reynolds stress tensor, which is probably partially responsible for the overall improved comparison with the experiment. However, as shown later, neither the multiscale model nor any of the other methods model the low-frequency unsteadiness of the separated flowfield. In this sense, as discussed later, the matching of the upstream influence by the multiscale model is partly fortuitous.

Unsteadiness

In the early 1960's, Kistler[12] made measurements of fluctuating wall pressures in turbulent interactions generated by forward facing step flows at Mach numbers of 3 and 4.5, and noted that the separation shock was unsteady. The unsteadiness was at relatively low frequency (or order 1–3 kHz), and has since been observed in many other turbulent interactions, such as those generated by blunt and sharp fins, circular cylinders, and compression ramps. A recent review of many of these studies is given in Ref. 13. A typical wall pressure signal in the region between the upstream influence line UI and separation line S (as deduced from surface tracers) in a Mach 5 compression ramp interaction is shown in Fig. 2. The dashed line is the mean of the signal and is the value that a conventional pressure tap would indicate. Currently, the unsteadiness is not modeled computationally and its neglect may be responsible for the discrepancies between the measured and predicted pressure distributions in Fig. 1. The discrepancy is consistent with the computed flowfield having a stationary separation shock stronger than the unsteady shock seen in experimental studies. Although the predicted shock is stationary the streamwise pressure gradient in the computation is not abrupt because the pressure rise across the shock is spread over a few grid points.

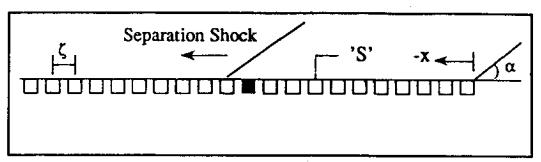

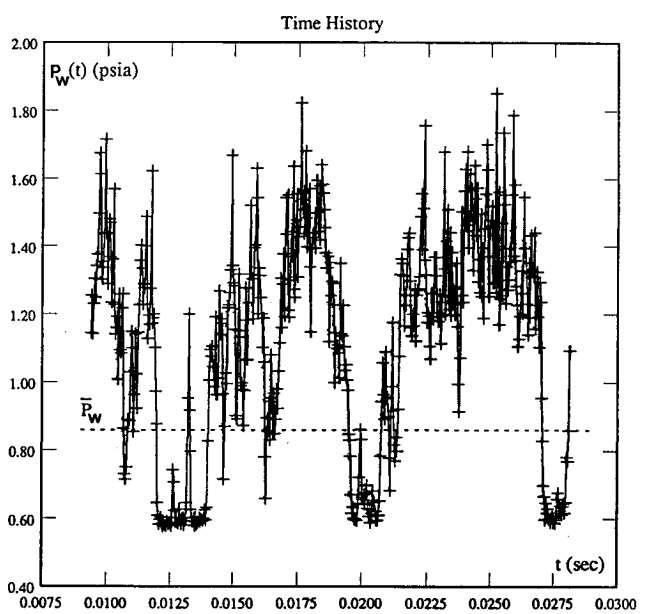

Fig. 2 Wall pressure signals in the intermittent region of a 28 deg, Mach 5 compression ramp interaction.

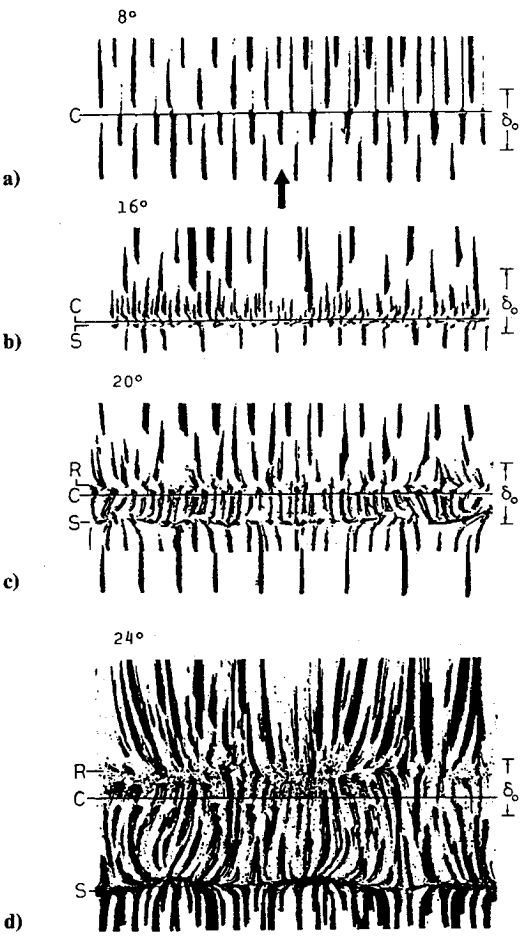

Fig. 3 Kerosene-lampblack surface tracer patterns for 8, 16, 20, and 24 deg, Mach 3 compression ramp interactions.[14] (S, R, and C denote separation, reattachment, and the ramp corner, respectively.)

Two-Dimensionality

It is commonly assumed that unswept compression ramp interactions are two-dimensional, despite some experimental evidence to the contrary. The surface flow visualization of Settles, et al.[14], reproduced in Fig. 3, shows that as the separated bubble grows, a well-defined spanwise pattern develops. Whether the structure causing it is buried deep in the boundary layer and manifests itself only in small changes in wall shear stress (which drives the surface tracer material) leaving most of the boundary layer largely unaffected is not clear. To the authors' knowledge this question has not been examined, at least not in supersonic turbulent flows.

In microsecond schlieren photographs, the separation shock wave displays a layered appearance that has been attributed to spanwise rippling. Muck et al.[15] recently presented wall pressure signals measured simultaneously using transducers spaced 0.23 δ_0 apart and aligned spanwise under the unsteady separation shock in a Mach 3 compression ramp flow. The pressure signals showed that the separation shock had spanwise ripples with a wavelength as small (if not smaller than) 0.23 δ_0 and as large (if not larger than) 0.69 δ_0. In a later study of a 28-deg compression ramp flowfield at Mach 5, Nordyke[16] made similar measurements but using two trans-

ducers. One was fixed close to the tunnel centerline and the other was moved spanwise in increments of about 0.17 δ_0. The maximum spanwise scale of the shock front ripple wavelength was estimated to be about 2 δ_0. Plots of the coherence function showed that at these large spacings only the lowest shock frequencies remained coherent.

Study Objectives

In the current study the objective was to determine if the discrepancy between experiment and computation upstream of the corner for such nominally two-dimensional flows is more likely due to the flowfield unsteadiness or its three-dimensionality, rather than inadequate turbulence modeling. To examine this question, wall pressure fluctuations have been measured using streamwise and spanwise lines of pressure transducers upstream of a 28-deg unswept compression ramp in a Mach 5 flow. A "digital" analysis of the separation shock foot dynamics and an analysis of the time-averaged spanwise wall pressures has been made.

Experimental Program

Wind Tunnel and Model

The experiments were conducted on the test section floor of the 17.8 cm × 15.2 cm Mach 5 blowdown tunnel at the University of Texas in Austin. Kulite pressure transducers were flush mounted using a stereo microscope in a 8.26-cm-diameter brass floor plug. The plug had a row of 26 transducer ports on centerline and a second row of 8 ports parallel to and 2.92 mm from the centerline row. The transducer spacing, center-to-center, was 2.92 mm. The plug could be rotated to allow the transducer rows to be aligned streamwise or spanwise.

The model was a 28-deg unswept aluminum ramp, 3.81 cm high at the trailing edge and 12.7 cm wide, allowing 1.27 cm on either side for passage of the sidewall boundary layers. Aerodynamic fences were used to prevent spillage and to isolate the compression corner from sidewall boundary-layer effects. The transducer positions within the interaction were changed by moving the ramp relative to the floor plug. The maximum streamwise travel of the ramp was about 2.5 cm, thus, the change in incoming flow conditions was negligible. The test set-up and coordinate system are shown in Fig. 4. Upstream influence, separation, and reattachment locations are indicated by *UI*, *S* and *R*, respectively.

Instrumentation

Wall pressure fluctuations were measured with Kulite Model XCQ-062-50A (50 psia) and XCQ-062-15A (15 psia) pressure transducers. Each has an external diameter of 1.58 mm and a pressure-sensitive diaphragm with a diameter of 0.71 mm. The natural frequency of the diaphragm in the 50-psi transducer is 500 kHz, but a protective screen above it limits its response to about 50 kHz. The frequency response of the 15-psi transducer is similarly limited to about 50 kHz. The transducers were calibrated statically. Shock-tube tests have shown that static and dynamic calibrations differ by only a few percentage points.[17]

The output of the transducers was amplified by either PARC model 113, Measurements Group model 2311 or Dynamics model 7525 amplifiers. Gain settings were adjusted to give a maximum amplifier output of 7 volts for a pressure of 2.1 psi, the maximum value expected. After amplification, the signals were filtered by either Ithaco model 4113 or model 4213 filters. The lowpass cutoff was set to 50 kHz. The filtered signals were simultaneously digitized by the 12-bit A/D converter of a MASSCOMP minicomputer at a rate of 109.1 kHz/channel. One hundred records of data per channel (1 record = 1024 points) were taken. Noise on the data acquisition system varied from ± 6 to ± 18 A/D counts, resulting in signal-to-noise ratios from a low of 40, in the worst case, to more typical values of well over 100.

Flow Conditions

Total temperature and pressure in the tunnel setting chamber were measured with a chromel-alumel thermocouple and a Setra model 204 pressure transducer respectively. The incoming boundary layer and freestream properties were determined from pitot pressure surveys in a previous study.[16] The boundary layer undergoes natural transition well upstream of the test section. Freestream and boundary-layer properties using standard nomenclature are listed in Tables 1 and 2, respectively. $Z = 0$ is on tunnel centerline.

Test Procedure

Initially, measurements were made along a streamwise line using eight transducers sampled simultaneously. A spacing of 2.92 mm allowed an overall streamwise coverage of 2.05 cm. The objective was to locate the upstream and downstream boundaries of the region of shock wave unsteadiness (i.e., the intermittent region).

Spanwise measurements were then made using several transducer configurations. First, eight transducers were aligned in a single row at single (2.92 mm), double (5.84 mm), and triple spacing (8.76 mm), allowing spanwise coverages of 2.05 cm, 4.09 cm, and 6.13 cm, respectively. For the single spacing case, the first transducer was adjacent to the plug centerline. Thus, measurements could be made on either side of the tunnel centerline by rotating the plug 180 deg. Tests were made at various distances upstream of the ramp corner. A second arrangement involved two rows of four transducers aligned spanwise. The rows were 2.92-mm apart in the streamwise direction, while the spanwise spacing varied from 2.92

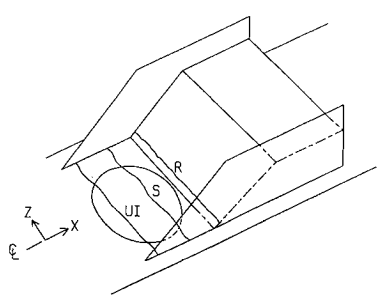

Fig. 4 Model and coordinate system. (UI, S, and R denote upstream influence line, separation, and reattachment, respectively.)

Table 1 Freestream properties

M_∞	4.95	± 1%
U_∞	774 m/s	± 1%
Re_∞	4.87×10^7/m	± 5%
P_0	2158 kPa	± 0.5%
T_0	344K	± 1%

Table 2 Boundary-layer parameters

Parameter	$Z = -2.54$ cm	$Z = 0$	$Z = -2.54$ cm
M_e	5.01	4.96	5.03
U_e (m/s)	774	772	774
δ_0 (cm)	1.76	1.76	1.76
δ^* (cm)	0.660	0.639	0.631
θ (cm × 10^2)	5.38	5.31	5.31
Π	0.37	0.30	0.26
H	12.3	12.0	12.3
Re_θ (× 10^{-4})	2.43	2.13	2.21
C_f (× 10^4)	7.57	7.97	7.83

mm to 5.84 mm. Tests were again made at various locations upstream of the corner.

Analysis Techniques

Statistical and spectral analysis routines were used to determine time-averaged values and frequency content of the signals. These routines are standard and are not discussed here. A conditional analysis algorithm, used to distinguish between shock-induced and boundary layer-induced pressure fluctuations is described briefly. Algorithms using the conditioned signals to investigate the instantaneous shape and motion of the separation shock foot are discussed in greater detail.

Conditional Analysis

The wall pressure signal in the intermittent region (see Fig. 2) has three components: 1) the high-frequency, low-amplitude fluctuations of the incoming undisturbed turbulent boundary layer; 2) the low-frequency, large-amplitude changes in the signal level caused by the unsteady separation shock wave; and 3) the high-frequency, high-amplitude fluctuations downstream of the shock. Because the shock motion was of primary interest, it was necessary to eliminate components 1) and 3). A two-threshold conditional analysis algorithm was used to do that. The signal conversion process is outlined below. Full details and results of sensitivity studies are given in Ref. 18.

Determination of the lower threshold T_1 and upper threshold T_2 is the first step of the conversion process. Both are calculated using the mean boundary-layer pressure $\overline{P}_{wo}$ and the standard deviation of the boundary-layer pressure fluctuations σ_{Pwo}. The mean boundary-layer pressure is determined by calculating the probability distribution of the fraction of the pressure signal between $\overline{P}_w - 3\sigma_{Pwo}$ and $\overline{P}_w + \sigma_{Pwo}$. The reasons for these choices are explained in Ref. 18. This signal range is divided into 100 intervals. Each data point in the signal is first then examined to determine which interval it falls in and a counter for that interval is then incremented. The pressure corresponding to the interval with the highest counter value is $\overline{P}_{wo}$. Once $\overline{P}_{wo}$ has been determined, σ_{Pwo} is calculated from the pressure fluctuations below $\overline{P}_{wo}$. In a sensitivity analysis of the effect of threshold levels on the shock zero-crossing frequency (shock crossings per second) reported in Ref. 18, it was determined that thresholds of $T_1 = \overline{P}_{wo} + 3\sigma_{Pwo}$ and $T_2 = \overline{P}_{wo} + 6\sigma_{Pwo}$ provided the best combination to distinguish shock wave induced fluctuations from those of the boundary layer. These values were used in the current study.

Having calculated T_1 and T_2 for a given run, the pressure signal is converted as follows. The conditioned signal is initialized to 0 and remains 0 until its value rises above T_2. This represents upstream passage of the shock wave and the conditioned signal is then set to 1. It remains 1 until the pressure falls below T_1. This indicates a downstream shock passage and the conditioned signal is then reset to 0 completing the shock passage cycle. The pressure signal is now represented by a sequence of 1s and 0s, where a 1 indicates that the shock is upstream of the transducer and a 0 indicates that it is downstream. The intermittency γ representing the percentage of time the shock is upstream of the transducer, is simply the number of 1s divided by the total number of points in the signal.

Shock Shape Algorithms

In order to investigate the shape and motion of the separation shock wave foot, the data files for the spanwise tests, each of which contained eight channels of 102,400 points, had to be reduced to a more manageable form. The algorithm "FRAMEMAKER" was developed to do that. It creates a "snapshot," or frame, by digitizing the instantaneous shock shape for each sampling interval.

The single-row cases are considered first. For each channel, it is determined from the conditioned signal whether the shock is upstream or downstream of the transducer. If the shock is upstream, the channel is assigned a value of two and if it is downstream, the channel is assigned a value of one. This results in eight numbers describing the location of the shock relative to each transducer. Employing a "connect-the-dots" type of approach, a snapshot of the shock shape can be obtained. This shape can be represented by a single number by multiplying the value of the first channel by 10,000,000, the second by 1,000,000, the third by 100,000 and so on. These values are then added to give an eight-digit number representing the instantaneous planview of the shock front. An example is shown in Fig. 5a. An actual shape is obtained only when the shock is moving across the row of transducers. If it is completely upstream of all eight transducers, the resulting number is 22222222. If it is downstream of all eight transducers, 11111111 results.

A similar procedure is applied to the double-row case. These configurations have four streamwise pairs of transducers, each pair separated in the spanwise direction. Considering one of the pairs, there are three possibilities for the shock location. It can be upstream of both transducers, downstream of both transducers, or between them. A one is assigned if the shock is downstream of both transducers, a two if it is between them, and a three if it is upstream of them. For example, if the conditioned signals of the two transducers were zero and one, respectively, indicating that the shock is between them, that pair is assigned a value of two. The remaining three pairs are evaluated in a similar manner. There are now four numbers representing the shock location relative to the transducers forming each pair. As before, they are reduced to a single number. The value assigned to the first pair is multiplied by 1000, the second by 100 and the third by 10. The value of the fourth pair remains unchanged. The four numbers are then

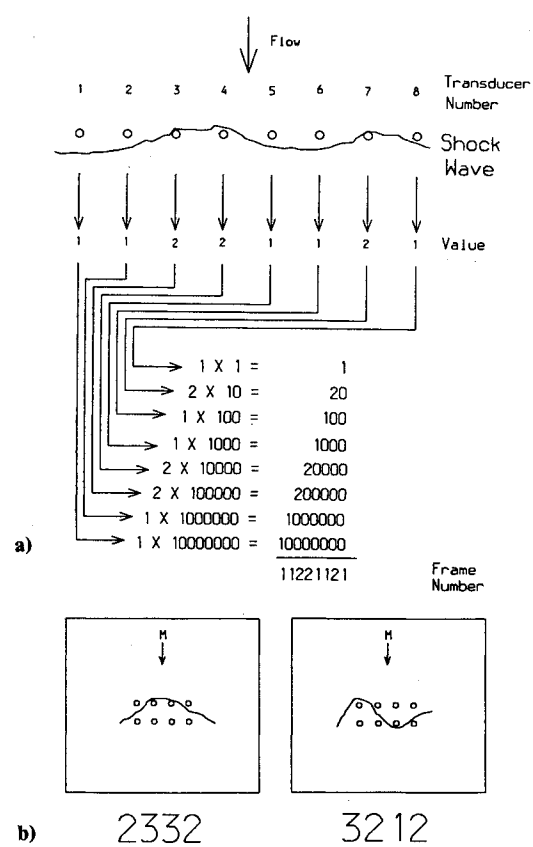

Fig. 5 Examples of shock shape conversion process: a) single row; b) double row.

added to produce a four-digit number representing the instantaneous shock shape for that sampling interval. Examples are given in Figure 5b.

This process reduces data files of 8 × 102,400 points to a single column of 102,400 numbers representing consecutive shock shapes. In essence, a 9.167 μs (sampling interval) frame-by-frame history of the shock as it passes over the transducer arrays has been developed. A histogram of the frames is then computed. Included in the histogram is the number of occurrences of each shock shape and its percentage of the total number of frames.

Frames of interest are then investigated with a pattern searching algorithm. The program PATTERN searches the entire file for every occurrence of the frame in question, which is input by the user. Every time this object frame is found, the frame following it is stored in an array. When the entire file has been searched, the array containing all of the subsequent frames is processed. The result is a list of frames that followed the object frame and the number of times each one occurred. The program also computes the maximum, minimum, and average times between occurrences of the object frame.

Because meaningful information is only obtained when the shock wave is in contact with the transducer array, an algorithm has also been developed to extract particular "blocks" of frames from the data file. Specifically, blocks of complete shock passages over the transducer arrays; that is, 11111111–22222222 for the single-row case and 1111 to 3333 for the double-row case, have been extracted because these contain information about the shock shape. In addition to visually inspecting these blocks for patterns and trends, a more quantitative analysis technique has been used. Three such blocks are shown in Fig. 6. In each block, each of the eight columns of digits is averaged giving a single frame of eight numbers ranging from approximately 1.0 to 2.0. If a complete shock passage is characterized by some channel having a high percentage of 2s, while channels on either side have a high percentage of 1s, then the "average" frame shape will have "crests" and "troughs," as in Fig. 6a and Fig. 6b. The distance between the crests (or troughs) defines the spanwise ripple wavelength λ. Of course, not all passages exhibit such a pattern. Fig. 6c shows an example where the shock is straight, but skewed.

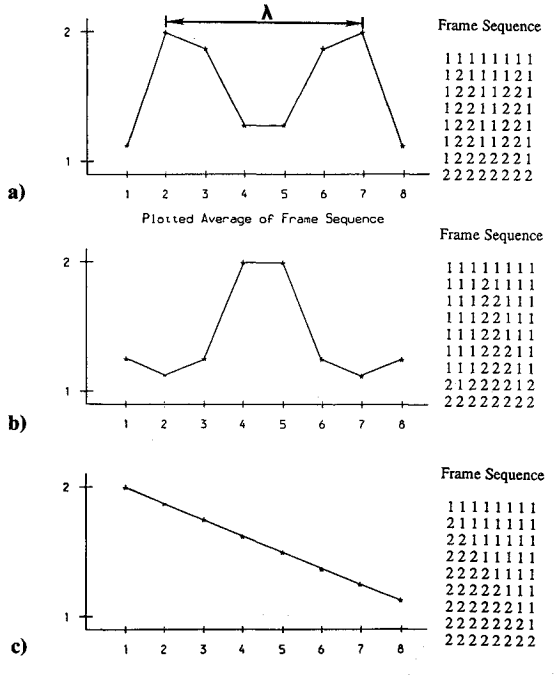

Fig. 6 Examples of shock passage frame averaging.

The inherent assumption is that the shock shape is essentially frozen while passing over the transducer array.

Results and Discussion

The time-averaged values calculated from spanwise data were used to evaluate the time-averaged two-dimensionality of the flow. Instantaneous data were then used to investigate the dynamics of the separation shock. The following questions were addressed: 1) Is the shock motion nominally two-dimensional with small-scale ripple amplitude, or is it a very "ragged" motion in which the shock may be at its upstream boundary at some spanwise position while simultaneously at another spanwise position it is at its downstream boundary?, 2) What are the largest, smallest, and average ripple amplitudes?, and 3) Is the motion random or is there evidence of a repetitive pattern?

Streamwise Results

The separation location "S" was deduced from surface tracer patterns and was at $X/\delta_0 \approx -1.25$. This provided the approximate location for the most downstream transducer, because "S" is just downstream of the limit of shock motion. At minimum spacing, the eight transducers spanned 2.05 cm, which covered practically the entire intermittent region. To assess repeatability, two runs were made with the downstream transducer 2.41 cm from the ramp corner. Figure 7 shows the intermittency distributions. For these runs, there is a systematic streamwise shift between the two curves, of about 0.1 δ_0 which, if interpreted solely as a length scale change, represents about 4% of the mean upstream influence. Part of the shift may be attributable to small variations in σ_{Pwo} due to electrical noise or randomness inherent in experimental measurements. Such small variations can alter T_1 and T_2 slightly, which influences the intermittency. This is a relatively small change and is not untypical of experimental measurements of intermittency. It can be seen from this figure that the shock motion length scale is approximately 1 δ_0 and extends from just upstream of "S" to the mean upstream boundary of the flowfield. Streamwise distributions of the shock-induced pressure rise ΔP ($\equiv \overline{P}_w - \overline{P}_{wo}$) and σ_{Pw} are shown in Fig. 8. In the case of ΔP, the mean pressure of the boundary-layer component is subtracted from the overall mean wall pressure in order to eliminate scatter from small zero shifts in the transducer output from run to run (induced largely by temperature changes).

The streamwise measurements also provided a means of evaluating the accuracy of the conversion of the raw pressure data into "boxcars" and then into frames. As the separation shock translates, it can be downstream of all eight transducers, in which case 11111111 is generated, it can be upstream of eight, giving a 22222222, or it can be between any two given transducers. If it is between #1 and #2121111111 is obtained. If it is between #2 and #3, 22111111 is obtained, and so on. Hence, for a line of eight transducers, only nine frames can

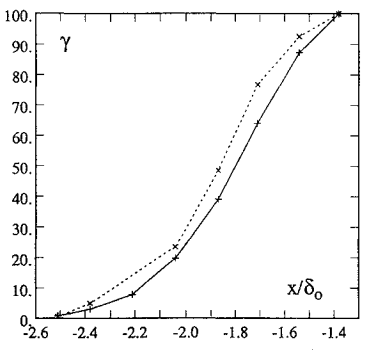

Fig. 7 Streamwise intermittency distributions.

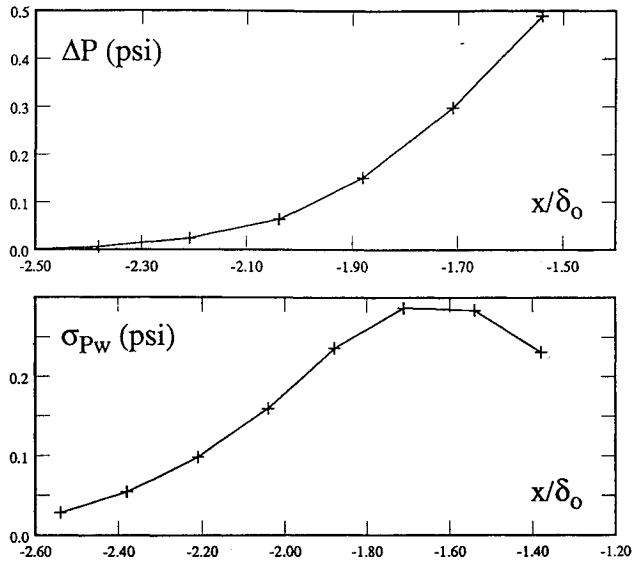

Fig. 8 Streamwise distribution of shock-induced pressure rise ΔP and wall pressure standard deviation σ_{P_w}.

physically exist; that is, 11111111, 21111111, 22111111, 22211111, 22221111, 22222111, 22222211, 22222221, and 22222222. As a test case, frames were generated from a run in which the downstream transducer was 100% intermittent and the upstream transducer had an intermittency of 0.8%. The histogram of the resulting frames contained only two frames (out of the 102,400) that were not possible. The frame 22,111,112, which occurred twice, is not physically possible. It is likely that electrical noise generated by some component of the data acquisition system was falsely registered as a shock. In summary, the number of "false" shocks is negligibly small, showing tht the two-threshold method of signal conversion is accurate and reliable.

Spanwise Results

Spanwise variations of intermittency, shock-induced pressure rise ΔP and wall pressure standard deviation at 2.79, 3.05, 3.30, 3.56, and 3.81 cm upstream of the ramp corner at various spanwise spacings were examined. Results for a spanwise transducer spacing of 8.76 mm (total span of 61.3 mm or 3.5 δ_0) are shown in Fig. 9. Recall that $Z = 0$ is the tunnel center-line. As expected, these triple-spacing cases showed the largest variations because they covered the largest span. Mean pressure rise and intermittency remain reasonably constant on the left side of the tunnel (looking upstream) and then drop off on the right side. In the case of the largest variation, the intermittency dropped from a maximum of 68.8% near the centerline to 44.6% 3.07 cm to the right of the centerline, while ΔP dropped from 0.31 psi to 0.19 psi. The standard deviation, which is calculated relative to the mean pressure of the channel and, thus, is not affected by zero shifts etc., is not entirely constant across the span but does not exhibit any repetitive spanwise trends. This is a very good indication that the flow can be considered reasonably two-dimensional in a time-averaged sense.

Power spectra in the form $G(f) \cdot f/\sigma^2_{P_w}$ versus f, where $G(f)$ is the power spectral density (psia^2/Hz) and f is the frequency are shown in Fig. 10. The eight curves shown are for triple spacing (total span = 6.13 cm $\approx$ 3.5 δ_0) and are at $X/\delta_0 = -1.7$ where the intermittency is nominally 65%. At a sampling rate of 109.1 kHz and with a data record length of 1024 points, the frequency resolution is about 106 Hz, and, consequently, the lowest frequencies are not well resolved. Nevertheless, it is evident that the shock motion is at low frequencies, typically less than 2–4 kHz with a large fraction

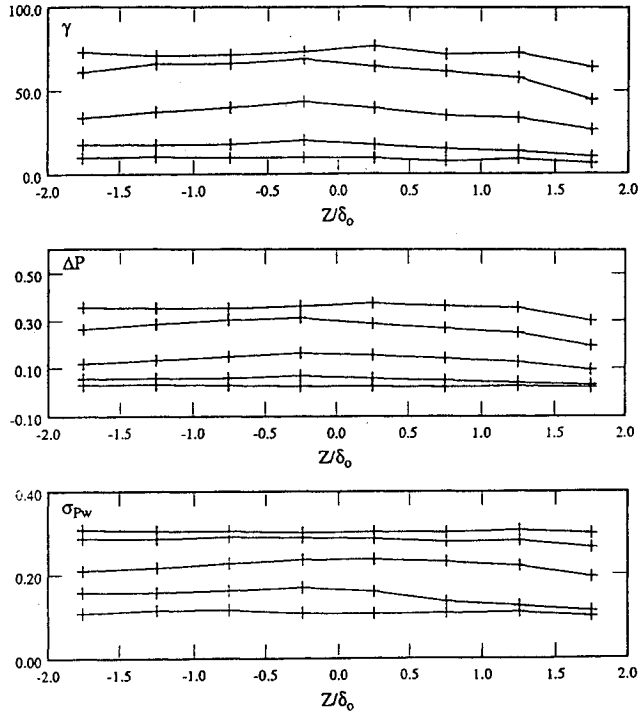

Fig. 9 Spanwise variation in intermittency, shock-induced, pressure rise and wall pressure standard deviation (transducers at triple spacing, ΔZ = 8.76 mm, $\approx$ 0.5 δ_0).

of the overall signal variance coming from frequencies below 1 kHz. The spanwise variation in $G(f) \cdot f/\sigma^2_{P_w}$ at any given frequency at maximum is about 10% about the mean value and there are no obvious trends. It is possible that the limited frequency resolution and the error incurred from calculating spectra from 100 records of data mask any trends, but should they exist they must be small. The coherence function between channels 1 and 2, 2 and 3, 3 and 4, etc. (seven curves in all) calculated from the same raw data as the power spectra of Fig. 10 are shown in Fig. 11. For triple spacing (8.76 mm $\approx$ 0.5 δ_0 between transducers), there is relatively little coherence due to turbulence, hence above about 4 kHz (the limit of the shock frequencies) the coherence is essentially zero. The high

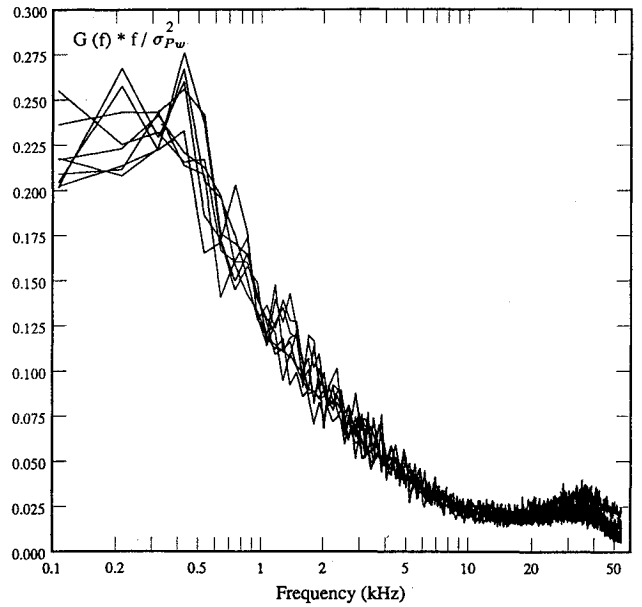

Fig. 10 Power spectra at eight spanwise stations for triple spaced transducers (all transducers located at $X/\delta_0 \approx -1.7$, $\gamma \approx 65\%$).

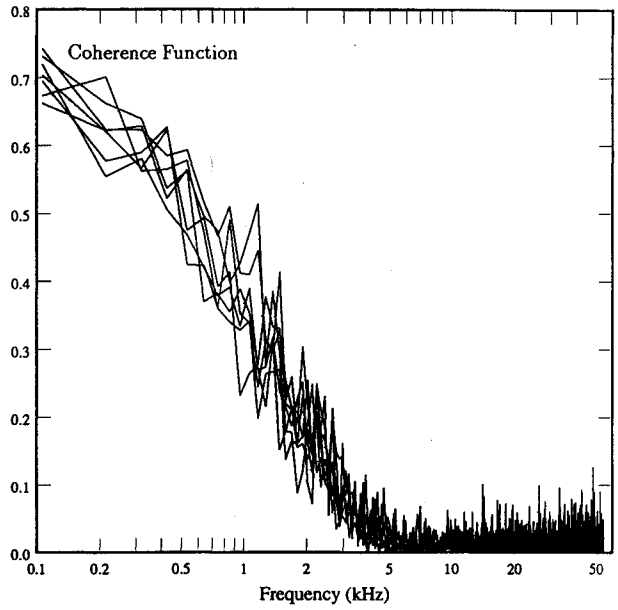

Fig. 11 Coherence function between channels 1 and 2, 2 and 3, 3 and 4, 4 and 5, 5 and 6, 6 and 7, 7 and 8 (same spacing and streamwise position as data of Fig. 10).

coherence at frequencies below 1–2 kHz is due almost entirely to shock-induced pressure fluctuations.

To learn more about the dynamics of the shock, three questions concerning its spanwise structure have been addressed using information obtained from analysis of the shock frames. (It should be noted that because of the large numbers of shock frames involved (102,400 frames per run for over 40 runs), it is difficult to present the data in a "reader friendly" format.) The first question concerns the amplitude of the ripples; that is, the streamwise distance from the leading edge of the shock foot to its trailing edge. Analysis has indicated that the shock undergoes a nominally two-dimensional motion with ripple amplitude typically less than 0.17 δ_0 (2.9 mm), as opposed to a motion with a large-scale amplitude spanning the entire length of the intermittent region. The best evidence of this comes from double-row transducer configurations. For these configurations, 2222 occurs when the shock is between the rows of transducers, limiting the maximum wavelength amplitude to 2.9 mm. From inspection of complete shock passages (1111–3333), there is a definite tendency to pass through 2222. For double-spacing cases spanning 1.75 cm, the shock passages generate the frame 2222 more than 50% of the time. For single-spacing cases spanning 0.876 cm, 2222 occurs about 70% of the time. Even when 2222 does not occur, a similar pattern (1222, 2122, 2232, etc.) usually does. Three blocks of actual shock passages illustrating this behavior are shown below. In this illustration successive duplication of frames has been eliminated and although time accuracy is lost, the pattern remains and is easily seen.

1111	1111	1111
2111	1112	1121
2211	1122	1222
2111	1121	2222
2211	1221	3222
2212	2221	3223
2222	2222	3233
3222	3222	3333
3322	3322	
3222	3332	
3223	3333	
3233		
3333		

Also, histograms reveal that 2222 is a very common frame, often third behind 3333 and 1111. These results are seen for both single and double spanwise spacing at all intermittencies tested. Frames indicating larger amplitude structures such as 1311, 1331, 1231, etc., do occur but are not nearly as common as those with smaller amplitude. These "large amplitude" frames generally account for less than a few percent of the total number of frames.

There is also evidence that the shock is more planar while moving downstream than while moving upstream. This is observed from pattern analyses of 2222, which represent a nominally two-dimensional condition. Frames representing downstream motion (2221, 1222, 2122, etc.) followed 2222 more often than for frames representing upstream motion. Sixty to sixty-five percent of the frames following 2222 are for downstream motion while only 30–35% are for upstream motion.

The second question involved the largest, smallest, and average wavelength λ of the ripples defined earlier in Fig. 6. Due to the finite minimum and maximum spacing, it is impossible to establish an absolute largest and smallest wavelength. For an entire ripple to be recognized, two "crests" must be detected. Consequently, the smallest wavelength that can be detected is 5.84 mm. This pattern, which occurs when a crest, trough, and crest are detected on three transducers at single spacing, was present, so that the smallest λ is 5.84 mm or smaller. Similarly, the largest ripple that can be detected, using triple spacing, is 4.38 cm. The necessary pattern for this wavelength was also found thus the largest λ is 4.38 cm or larger. The most important question concerning ripple wavelengths is whether an average exists and if it does, what is it? The averaging technique described in the previous section has been used to investigate this question. Figure 12 shows five possible shock foot shapes. Triple, double, and single transducer spacings along with their maximum detectable ripple wavelength λ_{max} are shown at the top of the figure. Below them, five possible shock wavefronts are given. The wavelengths of shock 1 are small enough to be detected by all three spacings. Shock 2 wavelengths are such that they are easily contained within the triple and double spacings, but would have to be perfectly aligned to register with the single-spacing arrangements. Shock 3 wavelengths are too large to be detected with single spacing and only rarely would they be detected with double spacing. A shock 4 wavelength could only be detected by triple spacing, and shock 5 wavelengths are too large to be detected at all. From an analysis of the single-spacing configuration at various intermittencies, entire ripple wavelengths are not generally seen (i.e., only single "crests" are detected). For double-spacing cases both entire ripples and single crest patterns are seen indicating that the

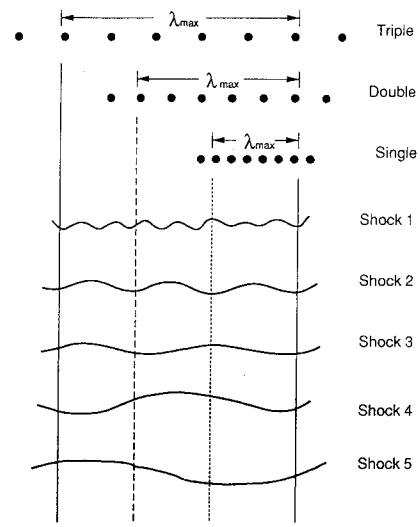

Fig. 12 Hypothetical shock foot shapes.

physical scale of complete ripples is being contained within the larger span. For triple-spacing cases single crest patterns practically never occur, indicating that very few complete ripple structures have wavelengths greater than 6.13 cm (triple-spacing span). All of this suggests that ripples of various wavelengths exist, but are typically larger than the single-spacing span (2.05 cm) and smaller than the triple-spacing span (6.13 cm) and quite often smaller than the double-spacing span of 4.09 cm. The shock front seems to lie somewhere between the hypothetical shock 2 and 3 in Fig. 12.

Additional evidence of the variety of ripple wavelengths comes from a more quantitative analysis of the averages of complete shock passages. For each passage, a ripple may or may not be present. If one exists, its wavelength is noted and saved. As previously discussed, very few wavelengths can be extracted from the single spacing cases, somewhat more for the double-spacing cases and a significant number from the triple-spacing cases. A histogram of the numbers of each wavelength does not produce a single preferred length, but rather a range from 0.58 cm (0.35 δ_0) to 3.5 cm (2 δ_0) with a slight emphasis around 1.75 cm (1 δ_0).

The third question is whether the spanwise shock structure is spatially and temporally random or if there is some preferable pattern. Analysis seem to indicate that the motion is random. This conclusion is drawn from pattern analyses of the frames 11111111 and 22222222. Because these frames indicate that the shock is completely downstream or upstream of the transducers, then from the frames that follow these, it can be seen how the shock first touches the transducer array. If there were a preferred or repeatable structure, it might be expected that the shock would first contact the transducer array near the same place every time or at least a high percentage of the time. This does not seem to be the case. The results of pattern analysis of 11111111 show that for single, double and triple spacing, the shock tends to first contact the interior transducers a relatively equal amount of time. The shock does, however, first contact the two outer transducers a higher percentage of time than the inner ones. This can be explained as follows. For the shock to register first on a particular interior transducer, the crest of the largest amplitude part of the shock foot has a definite spanwise range (which depends on spacing) through which to enter. The shock will register on either of the outer transducers as long as the shock crests on the outside of the array. This allows a much larger spanwise range and consequently, results in a higher percentage of occurrences. Similar results were obtained for the frame analyses of 22222222.

Flow Structure

The results show that the time-averaged wall pressure distribution under the moving separation shock front is essentially two-dimensional. The best evidence for this is the spanwise distributions of the wall pressure standard deviation. Unlike the intermittency, which is calculated using a conditional sampling technique whose thresholds depend on accurate resolution of the undisturbed boundary-layer pressure fluctuations, the standard deviation is calculated from the unprocessed raw signal. Spanwise distribution of wall pressure standard deviation is not constant, but there are no obvious spanwise trends for any of the spanwise spacings at any of the streamwise stations tested. A slight decrease on the right side of the tunnel is probably due to nonuniformities in the incoming flow. Thus, it seems that the periodic spanwise changes in the wall shear stress that generate the surface tracer patterns in Fig. 3 are not reflected in the time-averaged wall pressure, or the changes are too small to detect using this pressure measuring method. It is fair to conclude that for engineering calculations, little error is incurred by assuming a two-dimensional flow, and that a single streamwise pressure distribution on or off centerline is representative of the flowfield.

Analysis of the separation shock wave dynamics shows a rippled separation shock front. Because the flow upstream of the shock foot is the undisturbed turbulent boundary layer, the instantaneous upstream influence line has the shape of the shock front and varies continually. The shock front may also be considered nominally two-dimensional in the sense that the streamwise distance from its instantaneous leading edge to its instantaneous trailing edge is a relatively small fraction (about 0.2) of the length of the intermittent region. Because there is a low probability that the shock front ever spans the intermittent region, the most appropriate model is that sketched in Fig. 13. The ripple wavelength does not seem to have a preferred value, but falls in the range 0.35–2 δ_0. Finally, the motion seems to be temporally and spatially random.

Implications for CFD

The results above validate the two-dimensional assumption for the time-averaged wall pressure distribution. However, it is evident that the separation process is characterized by a spanwise rippling shock front that undergoes a large-scale, low-frequency streamwise motion. The evidence cited above indicates that the statistics at any spanwise station can be considered representative. The time-dependent behavior shows clearly how the time-averaged results are generated. It is the occasional presence of the unsteady shock at what is called the upstream influence line (UI) that first increases the mean wall pressure above the undisturbed value. Most of the time, the pressure at UI is the undisturbed value. Furthermore, the mean pressure rises downstream of UI because the translating shock spends an increasing amount of time upstream of stations nearer the separation point. What is, in an instantaneous snapshot, an abrupt pressure rise across the separation shock, is smeared out from UI to S in the time-averaged picture because of the motion.

Modeling the flowfield with a stationary separation shock *cannot* simultaneously generate the correct upstream influence (as usually defined) and the correct time-averaged pressure. Even if the upstream influence matches the experiment (as it does in several of the computations in Fig. 1), the pressure distribution is generally incorrect. This is because the stationary shock model essentially produces an instantaneous snapshot of the flowfield, in this case for the separation shock close to the upstream influence line. In contrast, in the experiment, the pressure at any given point is the weighted average of a series of instantaneous flowfields, each for the separation shock at a different streamwise position. This is evident in Fig. 14, which shows ensemble-averaged streamwise pressures $\bar{P}_{E/A}$, from the shock foot to the ramp corner, generated by "freezing" the separation shock at various positions in the intermittent region. These data were obtained by Erengil and Dolling[19] using the same ramp model at the same incoming flow conditions. In the schematic at the top of the figure, filled markers show the transducer positions. The symbol n represents the position of the shock in the intermittent region. The solid line is the time-averaged pressure distribution, obtained by averaging the pressure signals

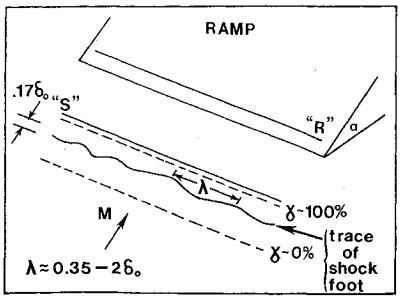

Fig. 13 Model of separation shock wave foot.

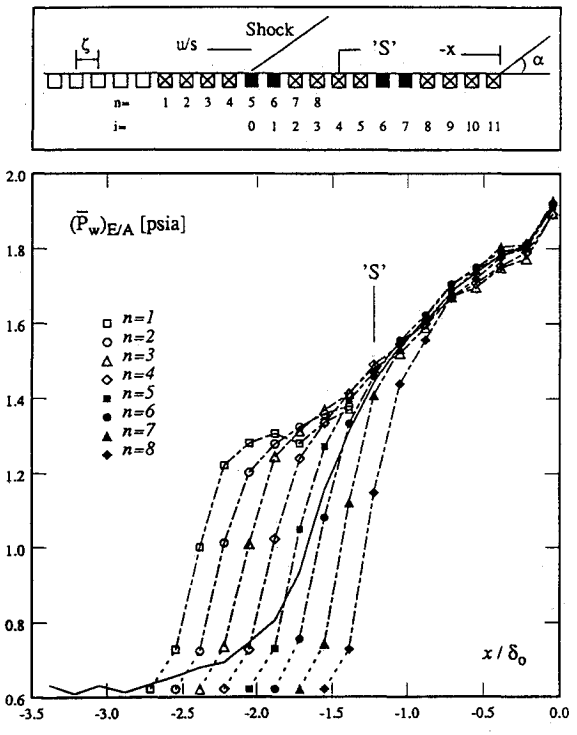

Fig. 14 Ensemble-averaged wall pressure distributions upstream of ramp corner (Ref. 19).

at each station. Clearly, time-averaged surface properties in an unsteady flowfield cannot be reproduced by a steady-state model. What is required is the inclusion of the translating shock front in the computational model. The problem is simplified by being nominally two-dimensional, such that spanwise rippling can be ignored. Time-averaging the computed wall pressures over many time-steps (as is done in the experiment) should substantially improve the comparison with experiment.

Summary

Examination of the literature shows that the comparison of experiment and computation for separated, supersonic, turbulent, unswept compression ramp flows is generally poor, irrespective of the turbulence model used. In the current experimental study, the objective was to determine if the discrepancy between experiment and computation might be attributable to the flowfield unsteadiness and/or its three-dimensionality, more than to inadequate turbulence modeling.

To examine this question, wall pressure fluctuations were measured using eight miniature pressure transducers in a 28 deg, separated, unswept compression ramp flow at Mach 5. The primary focus was the region under the unsteady separation shock wave. Measurements were made with the transducers oriented streamwise and spanwise for various transducer spacings. The conditionally sampled signals from the transducers were used to obtain "snapshots" or "digital frames" of the instantaneous separation shock foot as it passed over the spanwise array of transducers. Sequences of these frames were studied to determine the time-averaged and dynamic characteristics of the instantaneous separation shock front. The results show the following.

1) The time-averaged wall pressure field under the spanwise rippling, translating separation shock wave is essentially two-dimensional, validating one of the basic assumptions inherent in the computation of such flows.

2) The instantaneous separation shock front can also be considered two-dimensional in the sense that the ripple amplitude (i.e., the distance from the shock foot leading edge to its trailing edge) is a small fraction of the streamwise length of the region over which the shock translates.

3) Examination of the time-dependent behavior that generates the time-averaged wall pressure distribution upstream of the corner shows that such a distribution cannot be generated by a steady computation in which the separation shock is fixed in space, irrespective of the turbulence model used. Inclusion of the translating shock front in the computational modeling and then time-averaging the computed wall pressure values over many time-steps should substantially improve the comparison with experiment.

Acknowledgments

Support from AFOSR Grant 86-0112 monitored by Dr. L. Sakell and from the Center for Hypersonics Training and Research (supported by NASA, AFOSR, and ONR) is gratefully acknowledged.

References

[1]Knight, D., Horstman, C., Shapey, B., and Bogdonoff, S., "The Flowfield Structure of the Three-Dimensional Shock Wave Boundary-Layer Interaction Generated by a 20 Deg Sharp Fin at Mach 3," *AIAA Journal*, Vol. 25, No. 10, Oct. 1987, pp. 1331–1337.

[2]Knight, D. D., "Calculation of Three-Dimensional Shock/Turbulent Boundary-Layer Interaction Generated by a Sharp Fin," *AIAA Journal*, Vol. 23., No. 12, Dec. 1985, pp. 1885–1891.

[3]Hung, C. M., and Buning, P. G., "Simulation of Blunt Fin-Induced Shock Wave and Turbulent Boundary Layer Interaction," *Journal of Fluid Mech.*, Vol. 154, May 1985, pp. 163–185.

[4]Hung, C. M., and Kordulla, W., "A Time Split Finite Volume Algorithm for Three-Dimensional Flowfield Simulation," *AIAA Journal*, Vol. 22, No. 11, 1984, pp. 1564–1572.

[5]Knight, D., Horstman, C., Ruderich, R., Mao, M-F., and Bogdonoff, S., "Supersonic Turbulent Flow Past a Three-Dimensional Swept Compression Corner at Mach 3," AIAA Paper 87-0551, AIAA 25th Aerospace Sciences Meeting, Reno, Nevada Jan. 1987.

[6]Knight, D., Raufer, D., Horstman, C. C., and Bogdonoff, S., "Supersonic Flow Past A Swept Compression Corner," AIAA Paper 88-0310, AIAA 26th Aerospace Sciences Meeting, Reno, Nevada Jan. 1988.

[7]Viegas, J. R., and Horstman, C. C., "Comparison of Multiequation Turbulence Models for Several Shock Boundary-Layer Interaction Flows," *AIAA Journal*, Vol. 17, No. 8, 1979, pp. 811–820.

[8]Deese, J. E., and Argawal, R. K., "Shock/Boundary Layer Interaction in a Compression Corner," McDonnell Douglas Corp., MDRL 85-27, July 1985.

[9]Champney, J., "Modeling of Turbulence for Compression Corner Flows and Internal Flows," AIAA Paper 89-2344, *AIAA/American Society of Mechanical Engineers/Society of Automotive Engineers/American Society for Engineering Education 25th Joint Propulsion Conference*, Monterey, California July 1989.

[10]Wilcox, D. D., "Supersonic Compression-Corner Applications of a Multiscale Model for Turbulent Flows," *AIAA Journal*, Vol 28, No. 7, July 1990, pp. 1194–1198.

[11]Settles, G. S., "An Experimental Study of Compressible Turbulent Boundary Layer Separation at High Reynolds Numbers," Ph.D. Dissertation, Mechanical and Aerospace Engineering Dept., Princeton Univ., Sept. 1975.

[12]Kistler, A. L., "Fluctuating Wall Pressure Under Separated Supersonic Flow," Journal of Acoustical Society of America, Vol. 36, March 1964, pp. 543–550.

[13]Dolling, D. S., and Dussauge, J. P., "Fluctuating Wall Pressure Measurements," *A Survey of Measurements and Measuring Techniques in Rapidly Distorted Compressible Turbulent Boundary Layers*, Agardograph 315, May 1989, Chap. 8.

[14]Settles, G. S., Fitzpatrick, T. J., and Bogdonoff, S. M., "Detailed Study of Attached and Separated Compression Corner Flowfields in High Reynolds Number Supersonic Flow," *AIAA Journal*, Vol. 17, No. 6, June 1979, pp. 579–585.

[15]Muck, K. C., Dussauge, J. P., and Bogdonoff, S. M., "Structure of the Wall Pressure Fluctuations in a Shock-Induced Separated Tur-

bulent Flow," AIAA Paper 85-0179, AIAA 23rd Aerospace Sciences Meeting, Reno, Nevada Jan. 1985.

[16]Nordyke, R. J., "Spanwise Properties of the Unsteady Separation Shock in a Mach 5 Unswept Compression Ramp Interaction," Master's Thesis, Dept. of Aerospace Engineering and Engineering Mechanics, Univ. of Texas at Austin, Dec. 1987.

[17]Raman, K. R., "A Study of Surface Pressure Fluctuations in Hypersonic Turbulent Boundary Layers," NASA CR-2386, Feb. 1974.

[18]Dolling, D. S., and Brusniak, L., "Separation Shock Motion in Fin, Cyliner, and Compression Ramp-Induced Turbulent Interactions," *AIAA Journal*, Vol. 27, No. 6, June 1989, pp. 734–742.

[19]Erengil, M. E. and Dolling, D. S., "Separation Shock Motion and Ensemble-Averaged Wall Pressures in a Mach 5 Compression Ramp Interaction," AIAA Paper 89-1853, AIAA 20th Fluid Dynamics, Plasma Dynamics and Lasers Conf., Buffalo, New York June 1989.